

# **DROPWISE EVAPORATIVE COOLING**

**by**

**Marino di Marzo  
Mechanical Engineering Department  
University of Maryland  
College Park, MD 20817**

**Reprinted from ATTI 13 Congresso Nazionale Sulla Trasmissione Del Calore, 13 Unione Itallana Di Termofluidodinamica National Heat Transfer Conference, 22-23 Giugno, 1995, Bologna, Italy.**

**NOTE: This paper is a contribution of the National Institute of Standards and Technology and is not subject to copyright.**

# DROPWISE EVAPORATIVE COOLING

Marino di Marzo

Mechanical Engineering Department - University of Maryland  
College Park, MD 20817, USA

## ABSTRACT

A comprehensive review of the findings that punctuated ten years of research on dropwise evaporative cooling is presented. The first studies consider a single droplet evaporating on a high thermal conductivity solid surface. The solid-liquid coupling is addressed when considering the case of a low thermal conductivity solid. A powerful, non-intrusive, infrared thermographic technique is instrumental in describing the thermal behavior of the solid surface. The applications relevant to fire suppression suggest the input of radiant heat from above the surface instead of heat conducted through the solid. Once the single droplet behavior is fully documented experimentally and accurately modelled, the study of sparse water sprays is undertaken. A superposition model is formulated which well represents the experimental data.

## 1. INTRODUCTION

Evaporative cooling induced by droplets deposited on hot surfaces is of interest in a number of applications such as metal quenching, turbine blades cooling, and fire protection. The vaporization process depends on the degree of superheat of the solid surface. At high surface temperatures, the droplets float over thin vapor layers [1]. As the surface temperature is lowered, wetting occurs. The transition from the levitated state to the wetting state is known as the Leidenfrost transition. Since it was Leidenfrost who described the phenomenon in the first known two-phase heat transfer investigation which dates 1756 [2]. As the droplets wet the surface, nucleate boiling is observed. For lower surface temperatures, the bubble nucleation, at the liquid-solid interface, subsides and the vaporization occurs at the liquid-vapor interface. This process known as evaporation is the topic addressed here. As the surface temperature is further dropped, the vaporization rate is insufficient to remove the incoming water flux and the solid surface floods with liquid [3].

Extensive observations of a single droplet evaporation are available in the literature [4,5,6]. Modelling efforts available to date are based on a variety of simplifying assumptions and few address the behavior of sparse water sprays [7,8,9,10]. Most predictions are based on adjustments of constants fitted to the experimental data. The research presented here systematically progresses from the single droplet to the sparse spray. The heat input is at first by conduction from below the surface. Later, the heat is generated by radiant panels above the surface to simulate an environment closer to the typical fire protection applications. This paper parallels the experimental and the theoretical aspects and attempts to synergize the experimental observations with the insights provided by the theoretical results.

## **2. SINGLE DROPLET ON A SOLID HEATED BY CONDUCTION**

### **2.1 High thermal conductivity solids**

A spherical droplet impacting on a solid surface spreads on it. The final configuration of the liquid varies a great deal and depends on a multitude of parameters [11]. For the case of water gently deposited on a surface at near-saturation temperature, the shape can be regarded as a segment of a sphere [12]. The parameter  $\beta$ , defined as the ratio of the radius of the wetted region over the radius of the sphere of equivalent liquid volume [8] is sufficient to characterize the shape of deposited droplets of 10 to 50  $\mu\text{l}$ . For gently deposited water droplets on aluminum,  $\beta$  ranges between 1.2 and 1.5 as the surface temperature increases from 75 to 105 °C. For this experimental range, the radius of the wetted area remains constant throughout most (i.e. 90 percent) of the droplet evaporation time.

A simple model, based on one-dimensional conduction in the liquid, is proposed [13]. The temperature at the solid-liquid interface is assumed constant and uniform. Its value is estimated considering the contact temperature between two semi-infinite solids brought in sudden contact [14]. The temperature at the liquid-vapor interface is obtained from a heat and mass transfer energy balance for the steam-air mixture [15]. A spherical cap, based on the fixed radius of the wetted region and on the residual liquid inventory, describes well the transient droplet shape and defines the thickness of the liquid layer at each radial location from the center of the droplet.

The model is validated by comparing the calculated and measured evaporation times. These values agree within 10 percent. Further validation is achieved via photographic techniques. Figure 1 demonstrates the excellent agreement between the data and the computations. The model can provide insight into the flux distribution at the liquid-solid interface. Figure 2 shows the radial heat flux at various times during the transient. At first, the evaporation is taking place in the outer region of the droplet near its edge. Later in the process the whole surface contributes. This effect is clearly due to the variation in the thickness of the liquid layer which is associated with the decreasing curvature of the droplet liquid-vapor interface.

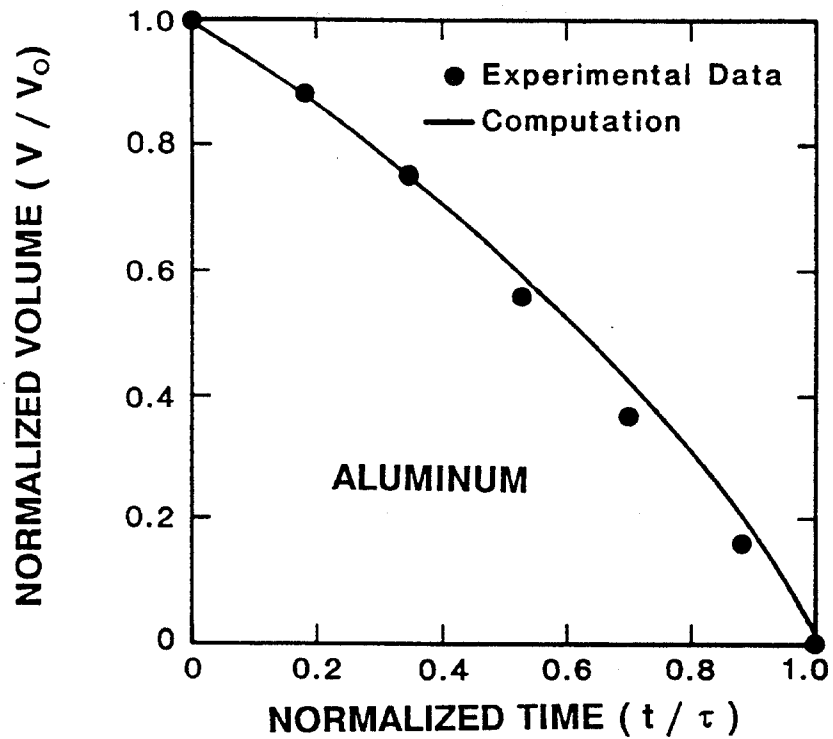


Figure 1. Liquid water inventory versus time ( $V_0 = 30 \mu\text{l}$ ;  $T_0 = 98 \text{ }^\circ\text{C}$ ).

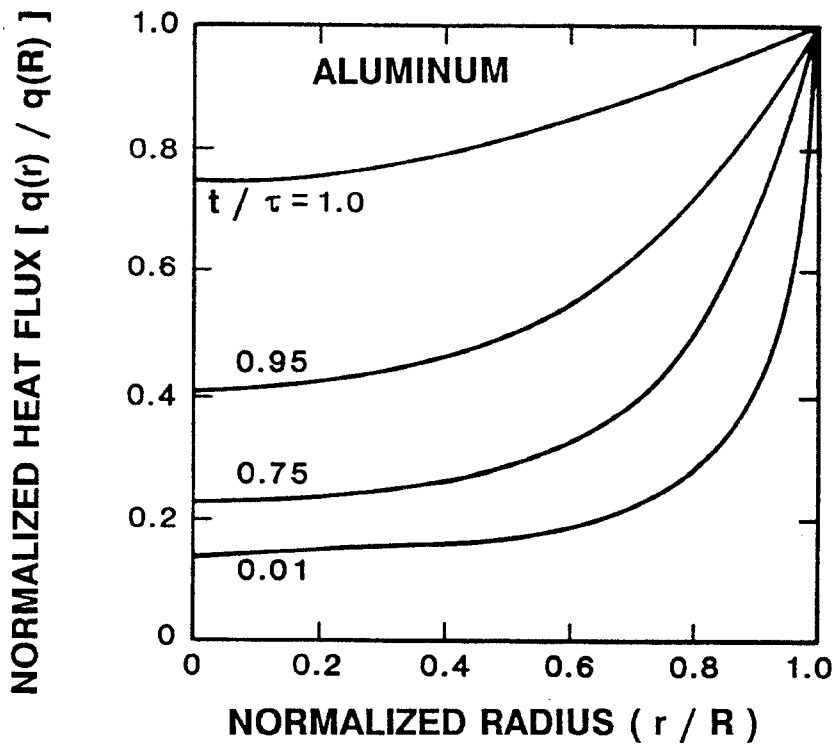


Figure 2. Temporal and spatial heat flux behavior ( $V_0 = 30 \mu\text{l}$ ;  $T_0 = 98 \text{ }^\circ\text{C}$ ).

The cooling effect on the solid surface is quantified by considering the heat flux distribution, due to the droplet evaporation, as a boundary condition in solving the semi-infinite solid transient conduction equation [16]. These studies demonstrate the adequacy of a simple conduction heat transfer model for the liquid layer. The hypothesis of negligible convective heat transfer is also supported by direct observation of the droplet with tracers and by studies of surface-tension-induced circulation [17]. Another important result is the validation of the liquid-vapor interfacial boundary condition casted in terms of a combined heat and mass transfer energy balance.

## 2.2 Generalization to low thermal conductivity solids

The previous work is extended to include solids with low thermal conductivity. The initial solid surface temperature is ranged from 90 to 180 °C with droplets of 10 to 50  $\mu\text{l}$ . The solid used for the experiments is Macor, a glass-like material. This solid has high emissivity which allows the use of infrared thermography to gather information on the transient thermal behavior of the solid surface [18]. An Inframetrics (Model 525) camera is used to capture the thermographic emission from the solid surface. The typical distance of the camera from the solid surface is of about 0.5 meters with a field of view of about 0.02 meters. The video signal from the camera is digitized by a PC-based frame grabber which converts the video image to a matrix of numbers representing gray levels. The gray levels identified by this equipment are 64 where 0 is black and 63 is white.

The image has infrared intensities on the vertical axis and radial positions, from the droplet center, on the horizontal axis. The digitized image is further processed by tresholding. This eliminates noise which is constituted by pixels of the digitized image with gray levels of less than 10. Additionally, an erosion technique is applied to verify the consistency of the data by checking if at least other six data points exist in the proximity of a given data point. To identify a reference temperature scale, the surface temperature is measured with an Omega surface probe (Series 68000) which is placed in the field of view. By comparing the temperatures read by the probe and the actual infrared images, immediately after the probe removal, the infrared intensity scale is associated with the temperature scale. Figure 3 illustrates a typical transient obtained with this procedure.

The extension of the model to the low thermal conductivity solids requires the introduction of the implicit coupling of the liquid and the solid whereas in the high thermal conductivity case (i.e. metal solids) the two could be treated separately. As observed in Fig. 2, the heat fluxes are significant at the droplet edge. This implies that the thermal gradients in the solid in the proximity of the droplet edge are very large. This fact precludes the application of a finite difference technique to integrate the solid transient conduction governing equation.

A different solution scheme is formulated for the solid region which is based on Boundary Element Methods (BEM)[19]. The BEM formally requires that all past information must contribute to the present solution. The advantage of the time

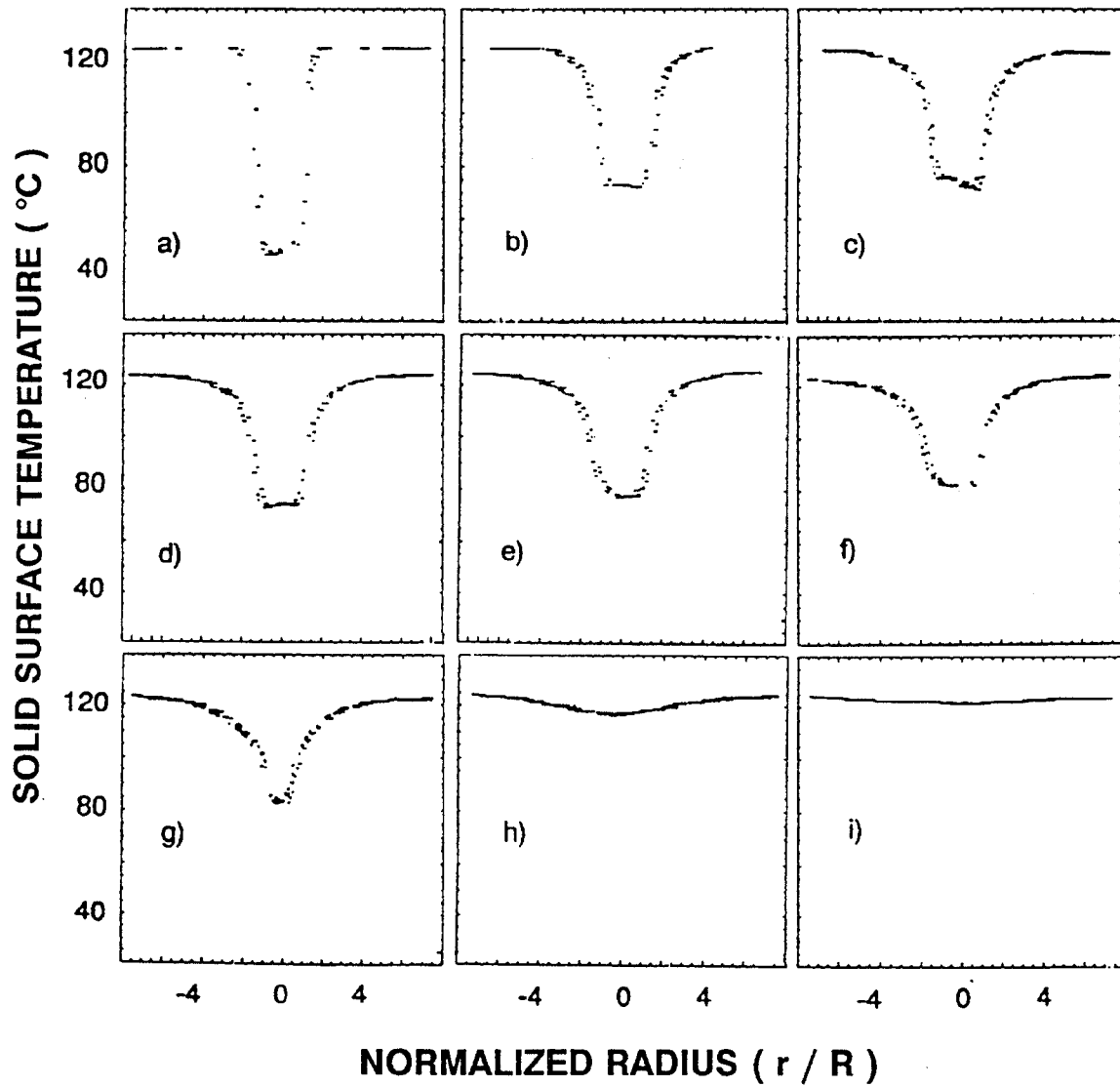


Figure 3 Evaporative cooling transient: a) at 1s; b) at 10 s; c) at 30 s; d) at 50 s; e) at 70 s; f) at 90 s; g) at 100 s; h) at 110 s; i) at 130 s ( $V_0 = 30 \mu\text{l}$ ;  $T_0 = 124^\circ\text{C}$ ; Macor).

discretization scheme used here, is that only a limited amount of past information must be collected in order to obtain the solution. The complex geometry of the liquid droplet suggests that a Control Volume Method (CVM) be used for the integration of the transient conduction equation in the liquid region. A simple nodalization scheme is used and the governing equation is discretized for each elementary control volume [20,21].

Figure 4 provides a comparison of the typical results of the model with the experimental data. Insights from the calculations are obtained for the temperature distribution at the solid-liquid interface. Figure 5 illustrate the dramatic difference between the behavior of high and low thermal conductivity materials. As it can be seen in this figure, the assumptions of the simple model for metallic solids finds clear supporting evidence in these results. For the low thermal conductivity case, it is clear that the temperature at the liquid-solid interface is not uniform nor constant. It is also important to point out that the transition to nucleate boiling occurs when the solid-liquid interfacial temperature exceeds saturation. Note that as soon as the droplet is deposited, the interfacial temperature drops significantly lower than the initial solid surface temperature. Therefore, while nucleate boiling on aluminum is observed for an initial solid surface temperature of 103 °C, it is necessary to reach about 164 °C to obtain nucleate boiling on Macor. The temperature distribution in the water layer is examined to assess the adequacy of a one-dimensional heat conduction model for the liquid region. Figure 6 compares the axial and radial components of the heat flux. Only at a few locations near the edge of the droplet for limited times, the radial flux is comparable to ten percent of the axial flux. Therefore, the assumption of one-dimensionality which is used in the model for high thermal conductivity solids holds and it is retained in the following.

### **3. SINGLE DROPLET ON A SOLID HEATED BY RADIATION**

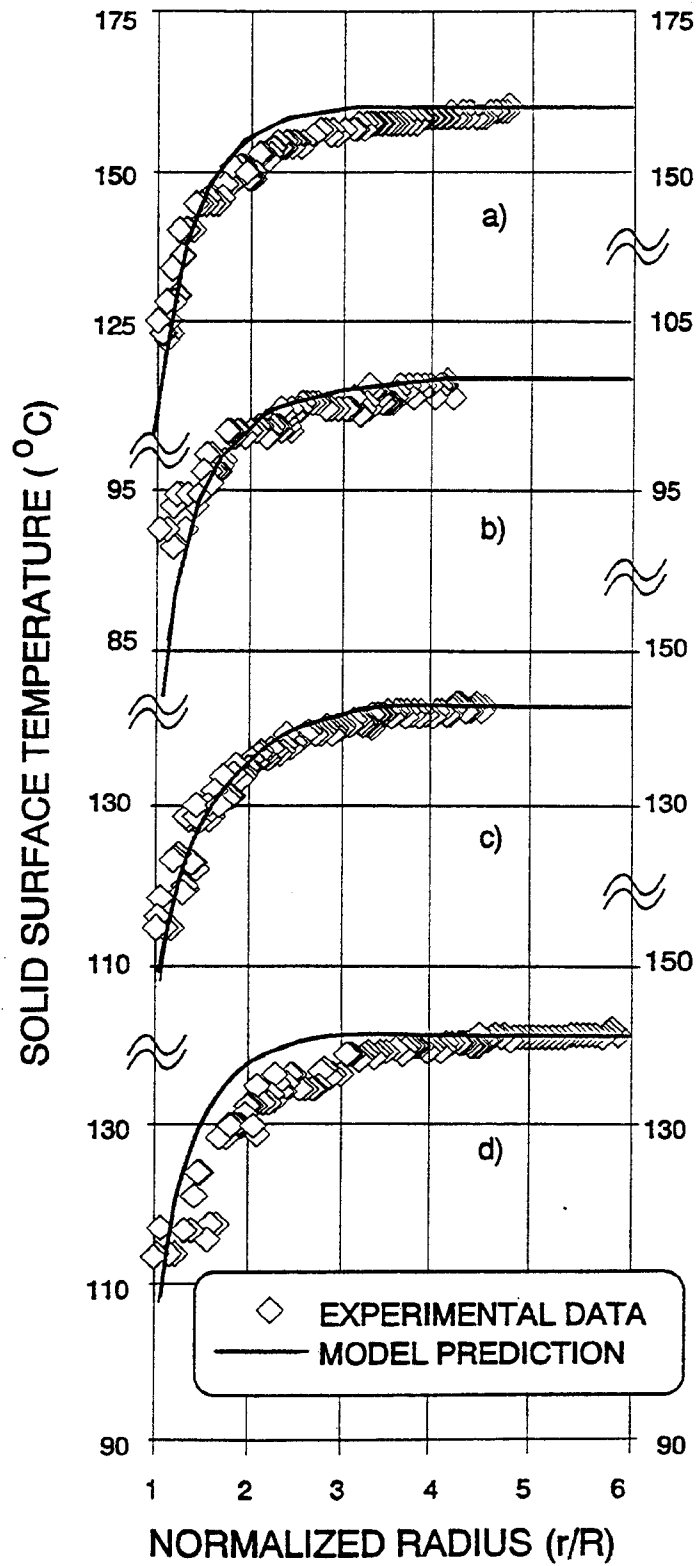
#### **3.1 Phenomenology**

In order to better approximate an actual fire environment, heat input by conduction from below the solid is substituted by radiant heat input from above the solid surface. The radiant heat input is provided by two conical shaped heaters positioned symmetrically with respect the solid surface [22]. The phenomena associated with the vaporization of a water droplet under these conditions is quite different from the previous case. Two major differences must be noted: a) the vaporization process is due to the direct heat input at the liquid-vapor interface in addition to the heat conducted from the solid surface through the liquid; b) the solid temperature distribution is the opposite of the previous case because the temperature decreases in the depth of the solid whereas before it was increasing. The temperature decrease in the depth of the solid is due to the radiant heat input from above the solid surface and to the use of a chilled plate at the lower surface of the solid to provide a constant temperature boundary condition. The effects of these two differences on the vaporization process are outlined in the following.

Figure 4

Model validation: solid surface temperatures for water on Macor at  $t/\tau = 0.9$  with:

- a)  $V_o = 30 \mu\text{l}$ ,  
 $T_o = 160 \text{ }^\circ\text{C}$ ;
- b)  $V_o = 30 \mu\text{l}$ ,  
 $T_o = 101 \text{ }^\circ\text{C}$ ;
- c)  $V_o = 10 \mu\text{l}$ ,  
 $T_o = 143 \text{ }^\circ\text{C}$ ; and
- d)  $V_o = 30 \mu\text{l}$ ,  
 $T_o = 143 \text{ }^\circ\text{C}$ .



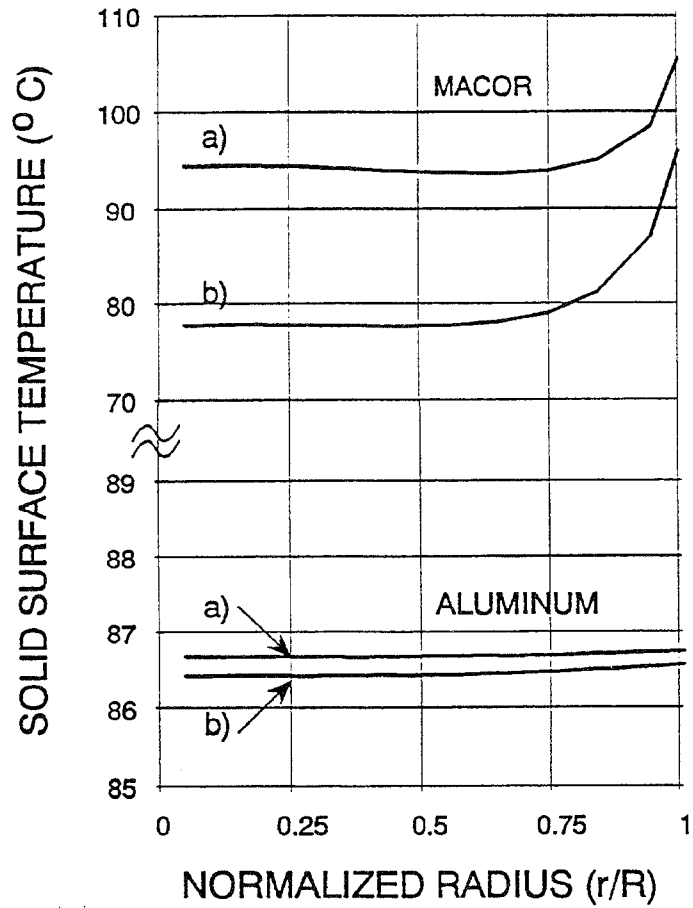


Figure 5 Typical liquid-solid interfacial temperatures for Macor and aluminum with initial contact temperature [14] of 82 °C for water droplets with  $V_0 = 30 \mu\text{l}$  at a)  $t/\tau = 0.3$  and b)  $t/\tau = 0.9$  (model computations).

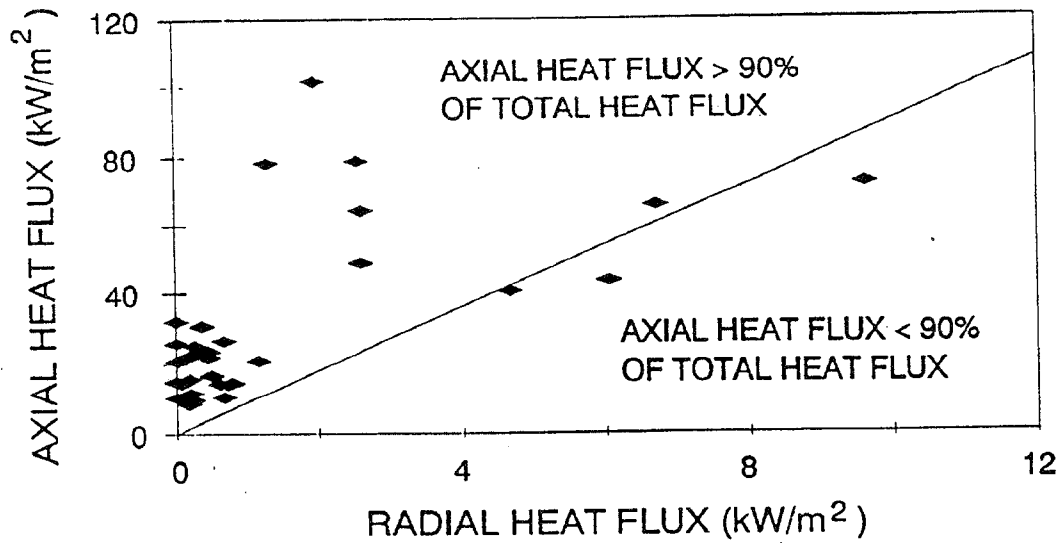


Figure 6 Calculated axial and radial heat flux components.

Figure 7 illustrates the behavior of the shape factor  $\beta$  as a function of the initial solid surface temperature. Note that the same material (i.e. Macor) exhibits values of  $\beta$  between 1.2 and 1.5 over the same range of temperatures for the case of heat input by conduction. The pronounced difference observed in these data is due to the effect of the direct radiant heat absorption at the liquid-vapor interface which increases the interfacial temperature and decreases the surface tension. The decrease in surface tension leads to a more pronounced initial spreading of the droplet on the solid surface. Note also that, as the nucleate boiling transition is approached (i.e. for temperatures of about 160 °C), the measurement scatter also increases. The increased spreading of the liquid on the solid surface implies that the liquid layer is thinner and, therefore, the resistance due to the heat conduction through the liquid layer is lessened. Another effect of the reduced thickness of the liquid layer at deposition is that the contact angle at the droplet edge is less than in the conduction case. As the droplet evaporates, the contact angle decreases from its initial value. There is a limiting value which is identified as the receding angle [23,24]. In this case the receding angle is between 7 and 10°. When this value of the contact angle is reached, the surface under the droplet starts shrinking and the liquid retains its aspect ratio while continuing to evaporate. Figure 8 clearly depict this occurrence. It is clear that as the initial value of the shape factor increases, the receding angle is reached sooner during the evaporative process, as it can be seen in the figure.

The other important difference has to do with the temperature distribution in the solid depth in relation to the cooling due to the droplet deposited on the solid surface. For the conduction case, the heat flux lines are converging from the hot depth of the solid toward the droplet. In the radiant case, the opposite is true since now the depth of the solid is cold. Therefore, as the surface cools, at the location of the deposited droplet, the heat flux lines diverge away from that region. The result of this opposite behavior is that the conduction heat input contribution to the vaporization process is far less than in the pure conduction case. The thinning of the liquid layer mitigate this effect and the vaporization by direct radiant heat input at the liquid-vapor interface compensate for the reduced heat input by conduction. The net result is a similar overall vaporization time which nonetheless is achieved by a substantially different mechanism.

### 3.2 Theoretical modelling

The first concern associated with the modelling of these complex phenomena relates to the estimate of the direct radiant heat input at the liquid-vapor interface. This estimate is based on the following description of the volumetric heat absorption in the depth  $z$  of a liquid layer of thickness  $\delta$  [25]:

$$H = 2 \int_0^{\infty} E_{\lambda} \kappa_{\lambda} \int_0^{\pi/2} \frac{1}{\mu} A_{\phi} \cos \phi \sin \phi (1 - \rho_{\phi}) e^{-\frac{\kappa_{\lambda}(\delta - z)}{\mu}} d\phi d\lambda \quad (1)$$

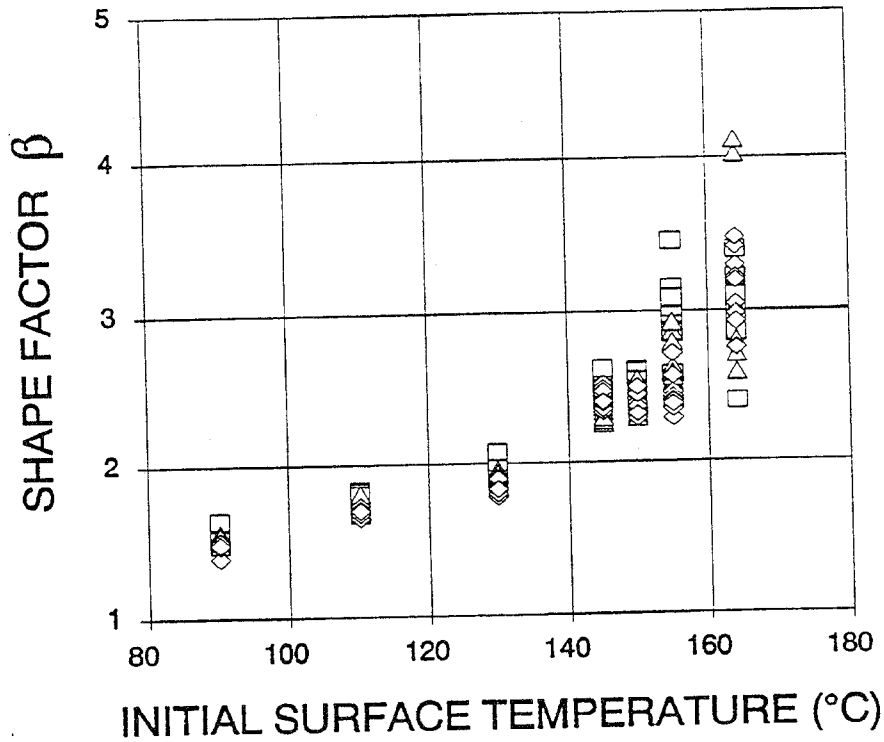


Figure 7 Shape factor:  $\diamond$ ) 50  $\mu$ l;  $\Delta$ ) 30  $\mu$ l;  $\square$ ) 10  $\mu$ l.

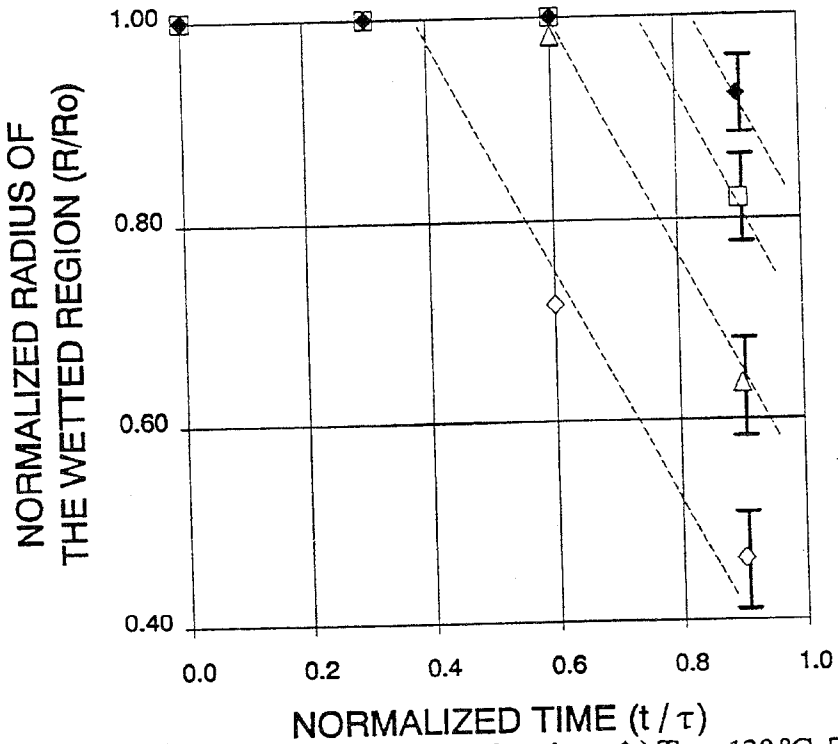


Figure 8 Normalized radius of the wetted region:  $\blacklozenge$ )  $T_0 = 130$  °C;  $\square$ )  $T_0 = 155$  °C;  $\Delta$ )  $T_0 = 164$  °C;  $\diamond$ )  $T_0 = 180$  °C.

Here, the geometry of the radiant heat source is identified in terms of the fractional surface area coverage occupied by the source,  $A_\phi$ , at various azimuthal angles,  $\phi$ , above the solid surface. The following assumptions are made: a) the radiant heat sources behave as black bodies; b) the radiation scattering within the water droplet is negligible; c) the liquid-vapor interface is horizontal and flat; and d) the radiation reaching the liquid-solid interface is completely absorbed by the solid. The absorption coefficient,  $\kappa_\lambda$ , is a very strong function of the wave length,  $\lambda$ , the direction cosine,  $\mu$ , is given by the Snell's law and the reflectivity,  $\rho_\phi$ , is less than 0.1 for  $\phi$  less than  $65^\circ$  and it is given by the electromagnetic theory.

Figure 9 shows that the volumetric heat absorption is high in a thin layer near the liquid-vapor interface (consider a layer thickness of about 0.05 mm). This is true over a broad range of the radiant surface temperatures. Therefore, one can split the direct radiation in three parts: a) an interfacial flux term (which is the integral of  $H$  over the thickness of a thin liquid layer); b) a volumetric heat absorption term which can be considered a constant, uniformly distributed heat source throughout the liquid layer; and c) a residual term which accounts for the incoming radiation at the solid-liquid interface. This last term is evaluated from an energy balance by deducting from the incoming radiant flux at the liquid-vapor interface the two previous terms. Careful consideration must be given to the fact that the liquid-vapor interface is not flat. The flat surface assumption is useful to obtain simple results as shown in Fig. 9. However, some error can be introduced in the evaluation of the total incoming radiation when significant radiant surfaces are present at large polar angles ( $\phi > 60^\circ$ ). To rectify this problem, a multiplier must be introduced which accounts for the liquid-vapor interface orientation given the transient geometrical configuration of the droplet.

The modelling of the droplet shape is a modification of the model based on a representation of the liquid layer as a segment of a sphere. The actual configuration is more flattened [11]. Two parameters are used to characterize the droplet shape at deposition: a) the contact angle,  $\theta$ ; and b) the shape parameter,  $\beta$ . The shape of the droplet, when the contact angle reaches its receding value, is assumed to be a segment of a sphere. This assumption is based on the minimization of the liquid-vapor interface which is consistent with the subsequent surface-tension-induced shrinkage of the droplet. Figure 10 illustrates the effect of the initial value of the contact angle. It is clearly shown that the receding angle is reached at about the same time during the transient. This means that the effect of the initial value of the contact angle has little or no effect on the overall phenomena. There is a compensatory effect in the droplet shape: a flattened shape has a uniform conduction heat input contribution while the spherical cap has very high heat transfer at the edge and far less heat transfer in the central region. The results shown here demonstrate that the overall effect is quite similar. Therefore, the simple model, based on the spherical cap configuration with the proper consideration for the receding angle, is adequate to represent the phenomena. The more complex two-parameters model is not used because there is no payoff from its increase complexity.

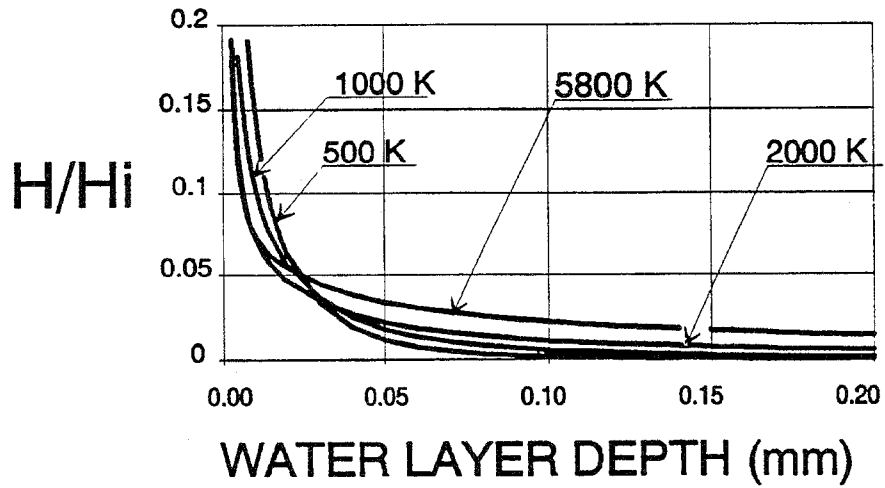


Figure 9 Normalized heat absorption in the liquid due to direct radiation.

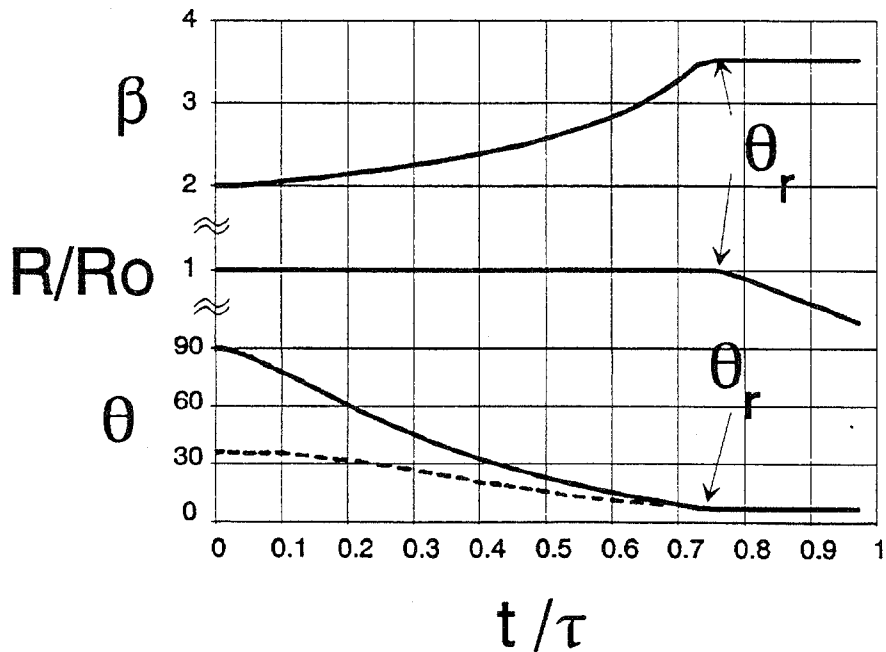


Figure 10 Transient behavior of the parameters governing the droplet shape ( $T_o = 130\text{ }^\circ\text{C}$ ;  $V_o = 10\text{ }\mu\text{l}$ ); — :  $\theta_o$  maximum - - - :  $\theta_o$  minimum.

The model for the direct radiant heat input and the new model for the transient droplet shape, which now includes the wetted surface shrinkage (as the receding angle is reached), are incorporated in the previous code for the coupled solid-liquid. Two independent versions of the same code are obtained. One of the codes is developed at the University of Bologna [26] and the other at the University of Maryland [27]. The code developed at the University of Bologna retains a full two-dimensional description of the liquid layer while the code developed at the University of Maryland uses a one-dimensional representation of the liquid layer transient conduction, as suggested by the results of the model for the conduction heat input case which were discussed previously. Both codes compared very well with the data. Figure 11 demonstrates the agreement between the infrared data and the calculated predictions.

#### 4. SPARSE SPRAY ON A SOLID HEATED BY RADIATION

##### 4.1 Experimental studies

A sparse spray is applied to a hot solid surface and the transient thermal response is monitored [28]. Figure 12 depicts the major components of the experimental apparatus. The solid surface is heated by three radiant panels. Two are positioned opposite to each other and the third is a low-aspect-ratio panel that surrounds the periphery of the solid surface. The infrared thermography is obtained with the same equipment previously described. Note that the camera observes the surface through a long chilled pipe to eliminate stray radiation and to avoid the direct reflection of the panels on the solid surface. The solid is chilled at its lower surface to achieve a controlled boundary condition. The sparse spray is obtained using a droplet dispenser capable of generating constant size droplets (the droplets volume is of about  $10 \mu\text{l}$ ) with a constant frequency which is set in the range from 1 to 0.1 Hz. The dispenser moves within a positioning plate which controls the droplet distribution.

Figure 13 shows a typical droplet distribution as measured via video-camera. The dispenser is positioned by three bumpers that periodically move in and out on the position plate. These bumpers randomly hit the dispenser which is suspended by four wires. The droplet distribution is characterized by a polynomial which is subjected to the following conditions in terms of the spray normalized radius,  $n$ :

- at  $n = 0$ ;  $f = 0$  and  $df/dn = 2$  which ensure that the distribution is proportional to the surface area (i.e.  $f \propto n^2$ )
- at  $n = 0.56$ ;  $df/dn = 0$  which sets a maximum value of the distribution at the radius bounding the region of free random motion of the droplet dispenser which is unconstrained by the bumpers motion (i.e.  $n = 0.56$ )
- at  $n = 1$ ;  $f = 0$  which insures that the outer maximum radial position is never reached
- the distribution  $f$  is normalized so that its integral over the whole spray region is set to unity

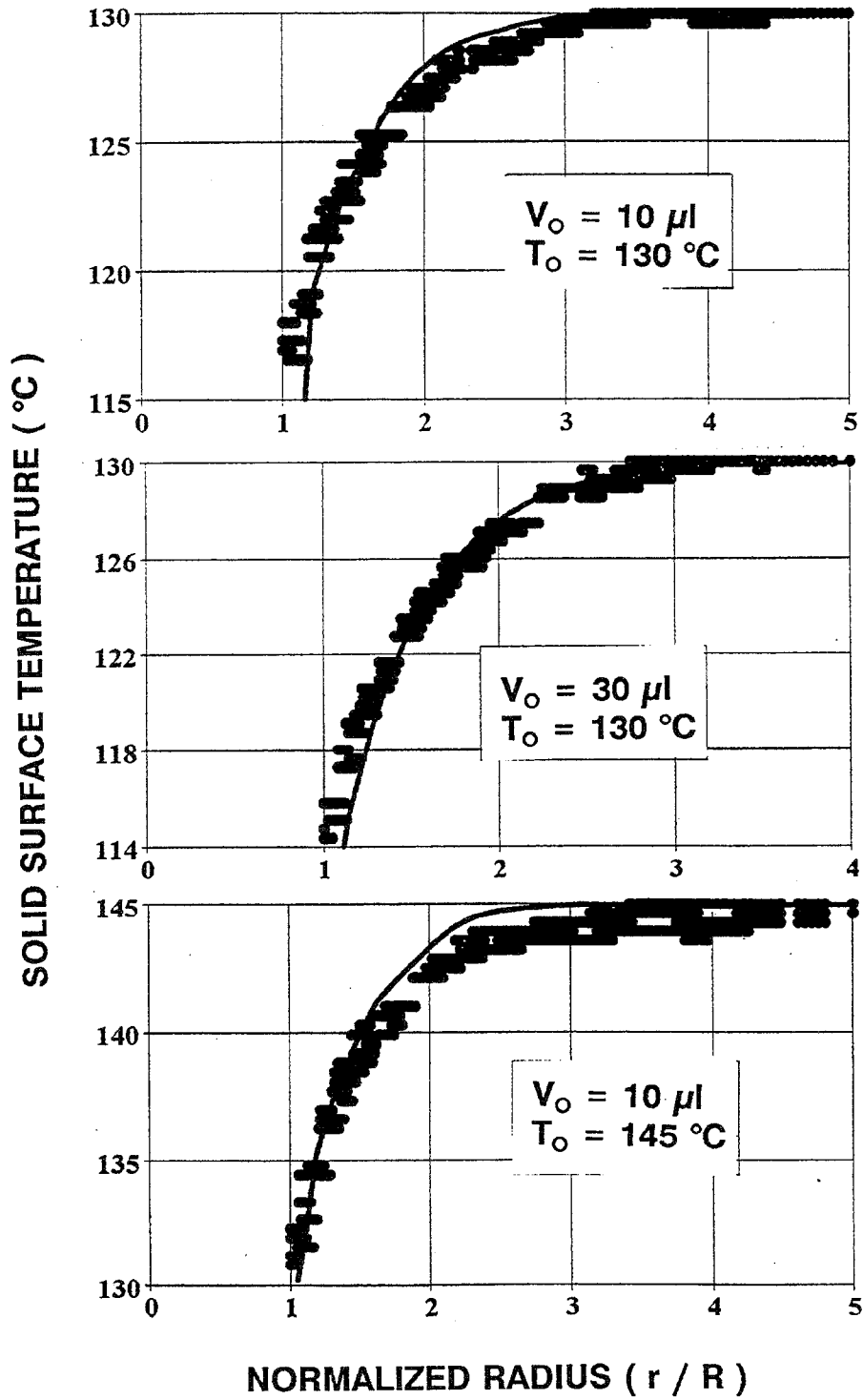


Figure 11 Model validation: solid surface temperatures for water on Macor at  $t = 0.3 \tau$  (— : numerical simulation; ■ : experimental data).

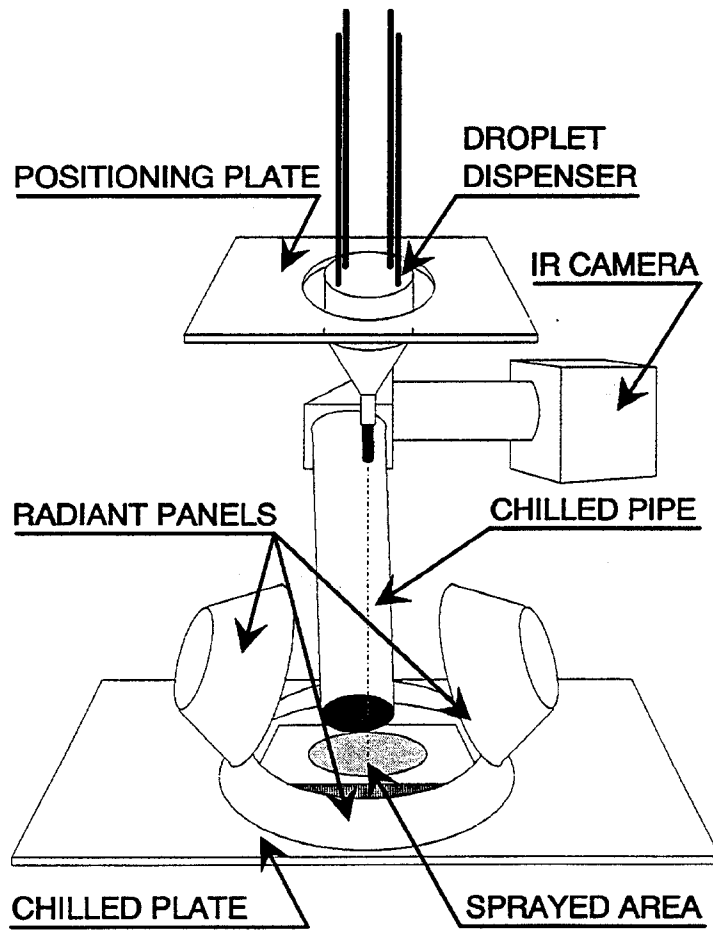


Figure 12 Experimental apparatus.

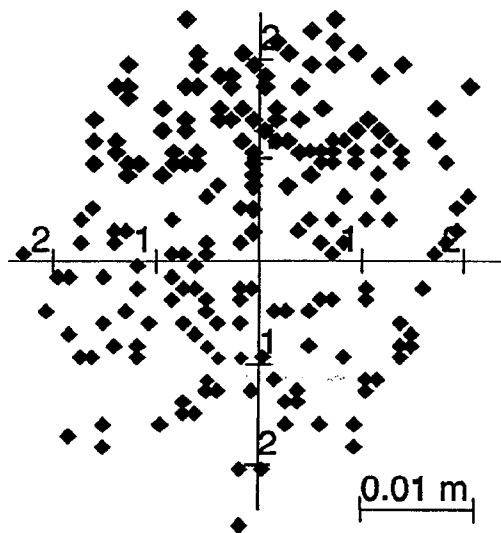


Figure 13 Typical droplet distribution.

With these conditions, the function  $f$ , describing the droplet distribution is given as:

$$f = 9.15 n^4 - 22.64 n^3 + 11.49 n^2 + 2.00 n \quad (2)$$

The integral of this distribution function is checked against the cumulative droplet distribution obtained from the figure and shows excellent agreement.

The infrared data is processed by a video digitizing system composed of a Matrox MVP-AT frame-grabber board installed in an IBM PC-AT. Once digitized, each frame is analyzed pixel-by-pixel using Image-AT software linked with a user-written source code. Figure 14 shows the typical data collected from an individual frame which is taken every 30 seconds during the transient. The overall experiments lasts about 15 minutes for a total of 30 frames. There are 130 shades of gray associated with the infrared intensity levels. Since the temperature range is of 100 °C, the temperature resolution is 0.77 °C/gray-value. A spatial resolution of 70 microns could be achieved. The data storage requirements limit the spatial resolution to about 0.5 mm. The gray value of every fifth pixel is used over an image covering a region 0.046 m x 0.034 m. For each frame, the temperature is averaged and a single data point is obtained. Figure 15 shows the typical transient behavior of the average surface temperature. The deviation of the data points from a smooth decay occurs due to the nature of the data acquisition. Since only a portion of the sprayed area is viewed and averaged, at any instant, the number of droplets that are in the field of view may be different than at other instants thus resulting in oscillations of the average temperature of the sampled surface. An exponential fit is used to curve-fit the data representing the transient behavior of the average solid surface temperature.

#### 4.2 Theoretical Model

The theoretical model for a sparse spray is based on the super position of the cooling effect of individual droplets [29]. Therefore, the temperature at a given point on the solid surface is the result of the combined effect of the cooling due to all the droplets previously deposited. In order to determine, in a compact form, the single droplet cooling effect, the droplets are subdivided in two groups depending on their proximity to the point of concern. The droplets outside a circular region of radius equal to five deposited droplet radii are considered in the far-field and their effect is reduced to that of instantaneous point sinks [30]. The droplets inside the previously defined circular region are considered in the near-field. Note that the size of the circular region is dependent on the cooling agent (i.e. water) and on the solid thermal properties (i.e. Macor). To seek a simple formulation of the cooling effect of a single droplet, one must study the effect of the solid-liquid interfacial boundary condition under the droplet [31]. Figure 16 shows the solid liquid transient boundary conditions calculated by the coupled code described previously in comparison with the closed form solution for the case of uniform and constant heat flux and for the for the case of uniform and constant contact temperature. The solution for uniform and constant temperature is discarded since it does not conserve energy. The solution for the case

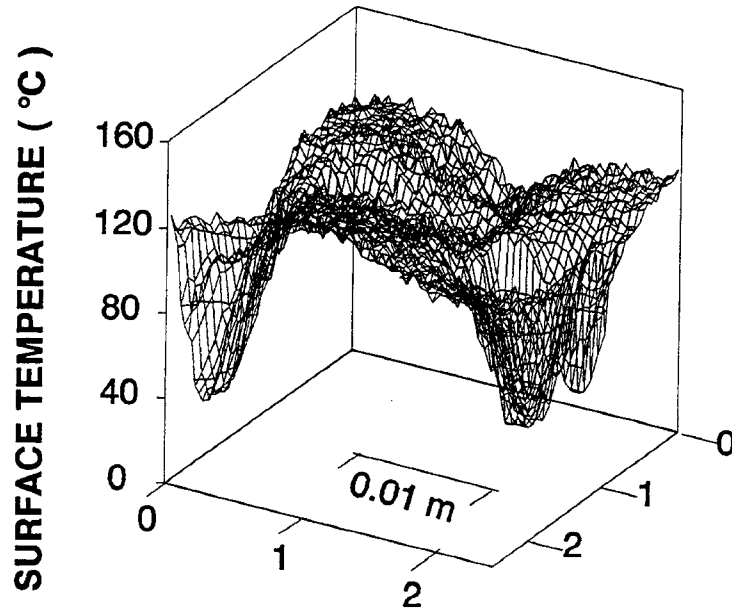


Figure 14 Typical surface temperature distribution for water on Macor (after 60 s;  $T_o = 140\text{ }^\circ\text{C}$ ;  $V_o = 10\text{ }\mu\text{l}$ ;  $G = 1.50\text{ g/m}^2\text{s}$ ).

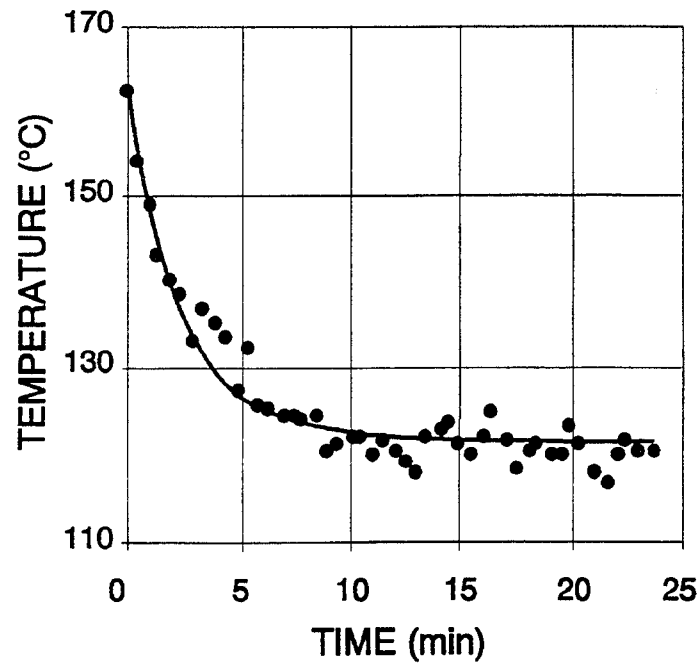


Figure 15 Transient average surface temperature ( $T_o = 162\text{ }^\circ\text{C}$ ;  $G = 0.97\text{ g/m}^2\text{s}$ ).

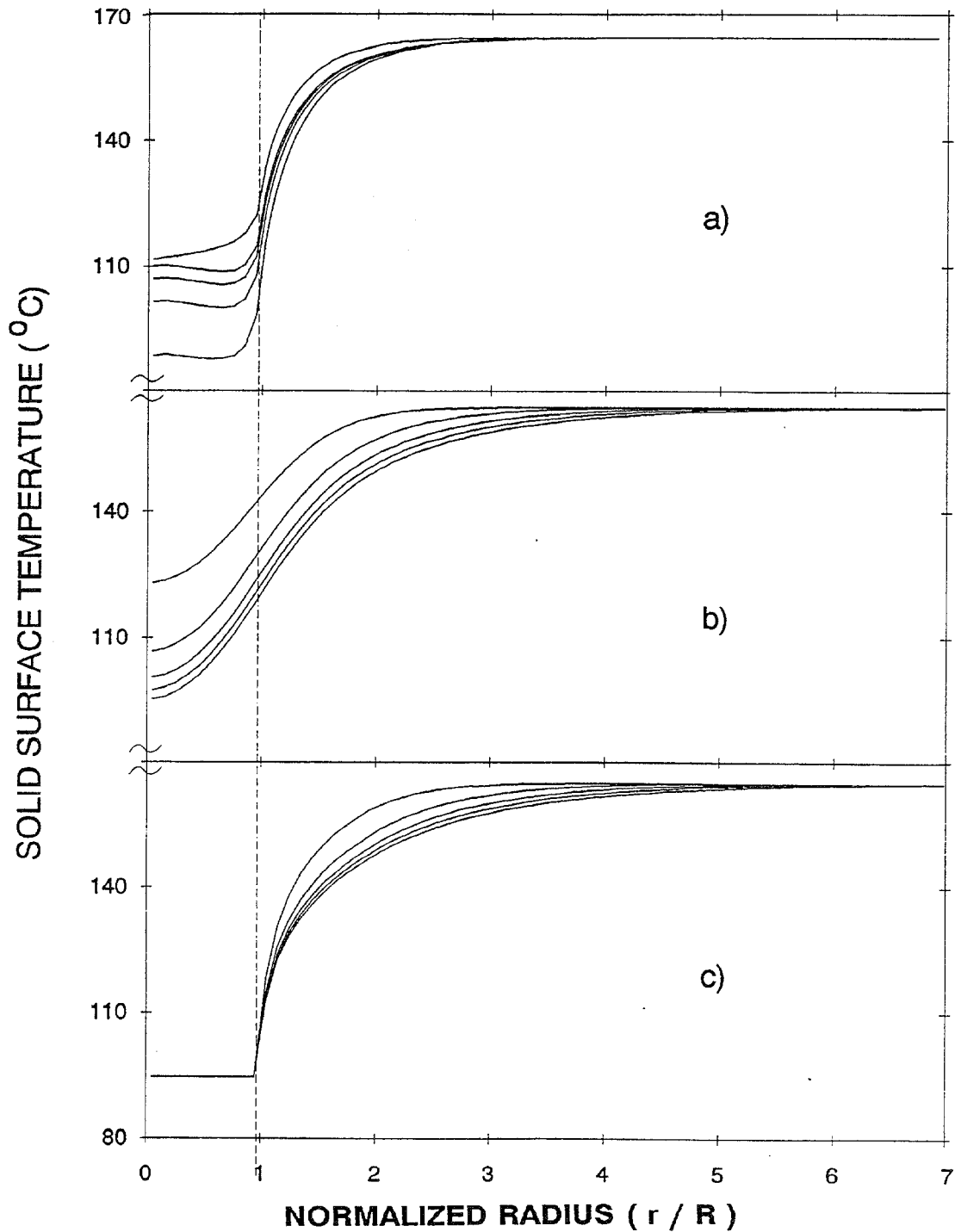


Figure 16 Typical solid surface temperature profiles for a  $10 \mu\text{l}$  water droplet on Macor with  $T_o = 165 \text{ }^\circ\text{C}$  at  $t/\tau = 0.1, 0.3, 0.5, 0.7$  and  $0.9$ : a) coupled code; b) code with constant and uniform heat flux; and c) code with constant and uniform interfacial temperature.

of uniform and constant heat flux is modified to include the recovery transient after the droplet evaporation is complete. The result can be written as:

$$T_o - T = \frac{q_o z}{k} + \zeta \frac{(q_c - q_o) R}{k} \quad (3)$$

$$\times \int_0^\infty J_o\left(\frac{\lambda r}{R}\right) J_1(\lambda) \left[ \operatorname{erf}\left(\frac{\lambda \sqrt{\alpha t}}{R}\right) - \operatorname{erf}\left(\frac{\lambda \sqrt{\alpha (t - \tau)}}{R}\right) \right] \frac{d\lambda}{\lambda}$$

The constant  $\zeta$  encompasses: a) the adjustment due to the shrinking of the wetted region; and b) the adjustment associated with the effect of the droplet curvature on the radiant heat input. This constant is set at 0.9 for the case of droplets of initial volume of 10  $\mu\text{l}$  over the range of initial solid surface temperatures from 70 to 164  $^\circ\text{C}$  which are bounding the experimental range under consideration. Note that the temperatures upper bound corresponds to the onset of nucleate boiling of water on Macor.

There are two inputs into the closed form solution which must be obtained from the single droplet code previously described. The fraction of vaporization heat input due to conduction from the solid (which is the heat flux  $q_c$ ) and the droplet evaporation time  $\tau$ . Both these quantities are function of the solid surface temperature at droplet deposition. With the near-field and the far-field solutions defined, the super-position of the cooling effects of all the droplets is evaluated for the point of concern. Note that the solid surface temperature at the location of deposition of each droplet must be known at the deposition time.

Figure 17 provides a comparison of the measured and calculated solid surface temperature distribution at two different times during the transient. Great care is taken to identify an identical portion of the spray area both in the model and in the computations. This is very important since just a portion of the spray area is seen and, therefore, the averaged surface temperature varies depending whether a central or peripheral field of view is considered. At the early stages ( $t = 50\text{s}$ ), the individual droplets are clearly defined by deep temperature drops at the deposition sites. This is evident for the experiment in the lower right end corner of the frame and for the mid-left region of the frame in the calculation. For both, the temperature excursion is between 80 and 140  $^\circ\text{C}$ . As the time progresses, the interactions of multiple droplet cooling effects become evident. Multi-droplet clusters are evident at 600 s in both the calculation and the data. Note the position of the isothermal at about 130  $^\circ\text{C}$  in both frames.

Figure 18 shows a comparison of data and calculations for a variety of cases in terms of the average solid surface temperature which has been normalized with respect to the initial solid surface temperature prior to the spray application and with respect to the final long-term steady state temperature evaluated by the model. There are

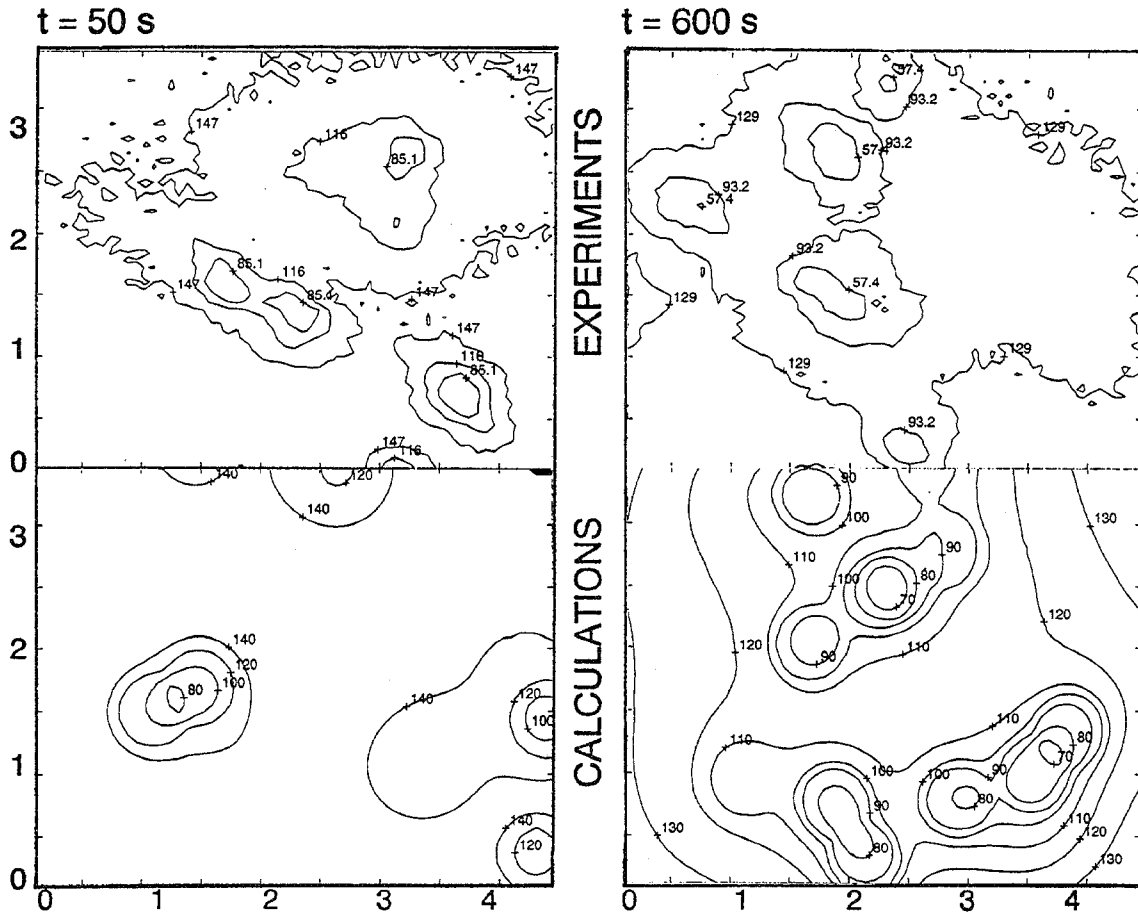


Figure 17 Typical transient surface temperature distributions ( $G = 0.96 \text{ g/m}^2\text{s}$ ;  $T_o = 151 \text{ }^\circ\text{C}$ ; distances on both axes in centimeters).

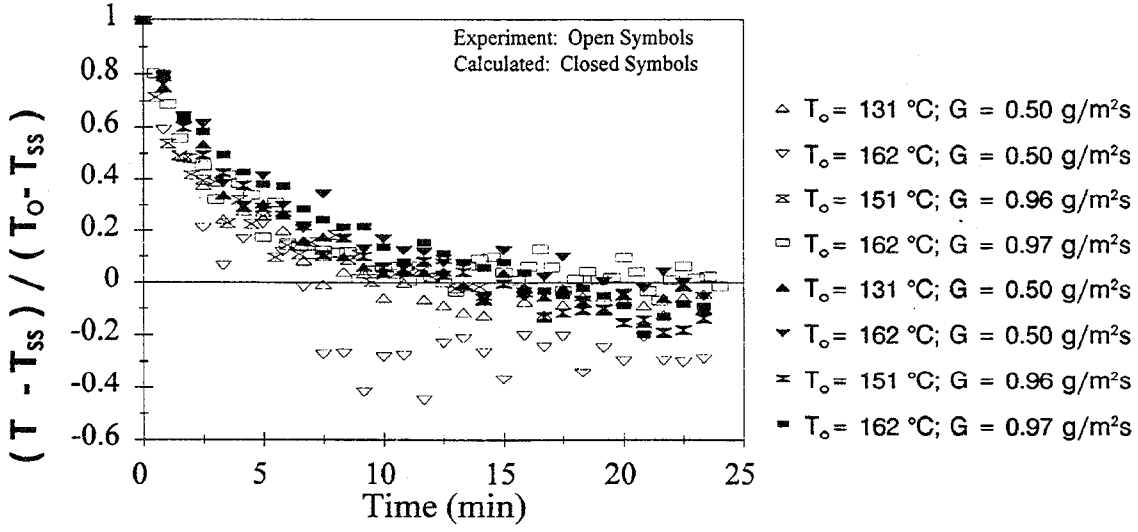


Figure 18 Summary of results: calculations versus experiments.

discrepancies between the calculations and the data for the set at 162 °C and  $G = 0.5 \text{ g/m}^2\text{s}$ . This is due to the occurrence of nucleate boiling in the early portion of the transient in the data. The model is limited to evaporative cooling and, therefore, it predicts a far less intense cooling. Note that, as the temperature of the surface drops, the data show a return to full evaporative cooling. However, the intense initial cooling due to nucleate boiling has deeply depleted the heat stored in the solid. It will take almost one hour for the system to recover the predicted steady state value in the experiment due to its large time constant. With this notable exception, the data and the computations agree very well. The independence of the surface cooling with respect to the water mass flux is evident. The substrate properties, that is the thermal properties of the solid, play a far more significant role. A cursory examination of the time constant and of the solid thermal diffusivity provides a value of the thermal penetration depth of the order of the droplet radius of influence on the solid surface. This quantitative correspondence can be used to estimate the overall response of solid surfaces subjected to spray cooling.

## 7. CONCLUSIONS

An overview of the research on dropwise evaporative cooling leading to the prediction of sparse spray cooling of hot solid surfaces has been presented. Early work on single droplets deposited on high thermal conductivity solids is used to validate the liquid-vapor boundary conditions and the assumption of negligible convective heat transfer in the liquid layer. The coupling of the liquid and the solid transient conduction equations allows the solution of the single droplet evaporating over low thermal conductivity solids and provides insight into the solid-liquid boundary conditions. The assumption of one-dimensionality of the conduction heat transfer in the liquid layer is also justified. Extension to the radiant heat input case is implemented by carefully evaluating the effect of direct vaporization of the liquid due to the radiant heat input absorption in the water layer. The differences between the conduction and radiant heat inputs are studied to gain in-depth understanding of the governing phenomena. With these models for the single droplet, the cooling effect of a sparse spray of uniform-size droplets is successfully evaluated. The average spray cooling is linked to the substrate properties (i.e. the solid thermal properties).

## ACKNOWLEDGEMENTS

The research was conducted at the Building and Fire Research Laboratory of the National Institute of Standards and Technology (BFRL-NIST). The guidance and support of Drs. Evans and Baum (BFRL-NIST) were essential to the performance of this work. The experiments and the analyses were performed by: Ham, Liao, Kavooosi, Kidder, Klassen, Mahajan, Meng, Tinker, Trehan, and White. The author wishes to thank Dr. Tartarini (University of Bologna) for his invaluable contribution over the last five years of this research.

## NOMENCLATURE

$A_\phi$	fractional area coverage	<b>Greek</b>	
$E_\lambda$	monochromatic emissive power	$\alpha$	thermal diffusivity
$f$	droplet distribution function	$\beta$	shape factor
$G$	water spray mass flux	$\delta$	liquid layer thickness
$H$	volumetric heat absorption	$\zeta$	constant; see Eq. (3)
$H_i$	limiting value of $H$ for $z \rightarrow 0$	$\eta$	integration variable
$J_0, J_1$	Bessel functions	$\theta$	contact angle
$k$	thermal conductivity	$\theta_r$	receding angle
$n$	spray normalized radius	$\kappa$	absorption coefficient
$q$	heat flux	$\mu$	direction cosine
$q_c$	conduction heat flux	$\rho$	reflectivity
$r$	radial coordinate	$\tau$	droplet evaporation time
$R$	radius of the wetted region	$\phi$	azimuthal angle
$T$	solid surface temperature		
$T_{ss}$	steady state surface temperature	<b>Subscripts</b>	
$V$	droplet volume	$o$	identifies initial conditions
$x, y, z$	cartesian coordinates		

## REFERENCES

1. K.J. Choi and S.C. Yao, Mechanism of film boiling heat transfer of normal impacting spray, *Int. J. Heat Mass Transfer*, **13**, 311-318 (1987).
2. J.G. Leidenfrost, *De aquaea communis nonnullis qualitibus tractatus*, (1756).
3. W.M. Grissom and F.A. Wierum, Liquid spray cooling of a heated surface, *Int. J. Heat Mass Transfer*, **24**, 261-271 (1981).
4. S. Inada, Y. Miyasaka and K. Nishida, Transient heat transfer for a water droplet impinging on a heated surface, *Bull. JSME*, **28**, 2675-2681 (1985).
5. C.O. Pedersen, An experimental study of the behavior and heat transfer characteristics of a water droplet impinging upon a heated surface, *Int. J. Heat Mass Transfer*, **13**, 369-381 (1970).
6. K. Makino and I. Michiyoshi, Discussion of transient heat transfer to a water droplet on heated surfaces under atmospheric pressure, *Int. J. Heat Mass Transfer*, **30**, 1895-1905 (1987).
7. S. Toda, A study of mist cooling. first report: Investigation of mist cooling, *Heat Transfer Jap. Res.* **1**, 39-50 (1972).
8. C. Bonacina, S. Del Giudice and G. Comini, Dropwise evaporation, *J. Heat Transfer*, **101**, 441-446 (1979).
9. J.J. Rizza, A numerical solution to dropwise evaporation, *J. Heat Transfer*, **103**, 501-507 (1981).
10. K.K. Tio and S.S. Sadhal, Thermal analysis of droplet spray evaporation from a heated solid surface, *J. Heat Transfer*, **114**, 220-233 (1992).
11. S. Chandra and C.T. Avedisian, On the collision of a droplet with a solid surface,

- Proc. Royal Soc.*, **432**, 13-41 (1991).
12. N. Zhang and W.J. Wang, Natural convection in evaporating minute drops, *J. Heat Transfer*, **104**, 656-662 (1982).
  13. M. diMarzo and D.D. Evans, Evaporation of a water droplet deposited on a hot high thermal conductivity surface, *J. Heat Transfer*, **111**, 210-213 (1989).
  14. M. Seki, H. Kawamura and K. Sanokawa, Transient temperature profile of a hot wall due to an impinging liquid droplet, *J. Heat Transfer*, **100**, 167-169 (1978).
  15. T.H. Chilton and A.P. Colburn, Mass transfer (adsorption) coefficients prediction data on heat transfer fluid motion, *Ind. Eng. Chem.*, **26**, 1183-1187 (1934).
  16. M. diMarzo and D.D. Evans, Dropwise evaporative cooling of high thermal conductivity materials. *Heat and Technology*, **5**, 126-136 (1987).
  17. S. Ostrach and A. Pradhan, Surface-tension induced convection at reduced gravity, *AIAA J.*, **16**, 419-424 (1978).
  18. M. Klassen, M. diMarzo and J. Sirkis, Infrared thermography of dropwise evaporative cooling. *Exp. Thermal Fluid Sci.*, **5** 136-141 (1992).
  19. L.C. Wrobel and C.A. Brebbia, A formulation of the boundary element method for axisymmetric transient heat transfer conduction, *Int. J. Heat Mass Transfer*, **24**, 843-850 (1981).
  20. M. diMarzo, Y. Liao P. Tartarini, D.D. Evans and H. Baum, Dropwise evaporative cooling of a low thermal conductivity solid. *Fire Safety Science - Proc. of the 3rd Int. Symp.*, ed. G. Cox & B. Longford 987-996 (1991)
  21. M. diMarzo, P. Tartarini, Y. Liao, D.D. Evans and H. Baum, Evaporative cooling due to a gently deposited droplet. *Int. J. Heat Mass Transfer*, **36** 4133-4139 (1993)
  22. M. diMarzo, C.H. Kidder and P. Tartarini, Infrared thermography of dropwise evaporative cooling of a semiinfinite solid subjected to radiant heat input, *Exp. Heat Transfer*, **5** 101-114 (1992).
  23. S.S. Sadhal and M.S. Plesset, Effect of solid properties on contact angle in dropwise condensation and evaporation, *J. Heat Transfer*, **101**, 48-54 (1979).
  24. F.F. Simon and Y.Y. Hsu, Wetting dynamics of evaporating drops on various surfaces, *NASA Tech. Memo. NASA TM X-67913* (1971).
  25. R. Siegel and J.R. Howell, *Thermal Radiation Heat Transfer*, Hemisphere Publishing Co., New York (1981).
  26. P. Tartarini and M. diMarzo, Dropwise evaporative cooling in a radiant heat field. *Proc. of the 10th Int. Heat Transfer Conf.*, ed. G.F. Hewitt, **6** 277-282 (1994).
  27. G. White, S. Tinker and M. diMarzo, Modelling of dropwise evaporative cooling on a semi-infinite solid subjected to radiant heat input, *Fire Safety Science - Proc. of the 4th Int. Symp.*, ed. T. Kashiwagi 217-228 (1994).
  28. H.F. Dawson and M. diMarzo, Multi-droplet evaporative cooling: experimental results. *AIChE Symp. Ser.*, **89** 26-35 (1993).
  29. S. Tinker and M. diMarzo, Multi-droplet evaporative cooling. *Annual Conference on Fire Research*, NISTIR 5499 69-70 (1994).
  30. H.S. Carslaw and J.C. Jaeger, *Conduction of Heat in Solids*, Clarendon Press, Oxford (1959).
  31. P. Tartarini and M. diMarzo, The solid-liquid interfacial conditions for dropwise evaporative cooling. *Heat and Technology*, **10** 130-144 (1992).